

PACS numbers: 42.55.Lt
DOI: 10.1070/QE2005v035n01ABEH002859

Generation of singlet oxygen for an oxygen – iodine laser in a radio-frequency discharge

O.V. Braginskii, A.N. Vasil'eva, K.S. Klopovskii, A.S. Kovalev, D.V. Lopaev, Yu.A. Mankelevich, N.A. Popov, A.T. Rakhimov, T.V. Rakhimova

***Abstract*. The generation of singlet oxygen (SO) in a radio-frequency discharge (13.56 MHz) in the gas flow was investigated experimentally and theoretically. The oxygen pressure was varied from 2 to 20 Torr and the energy deposition in gas from 10 to 2000 J mmol^{-1}. The saturation of the SO concentration with increasing the energy deposition was shown to arise from the three-body process of SO quenching by atomic oxygen. Removing atomic oxygen allowed a 2.5-fold increase in the ultimate SO concentration at the discharge output. For an oxygen pressure of 15 Torr, the SO fraction amounts to 10 %.**

Keywords: *singlet oxygen, oxygen – iodine laser, radio-frequency discharge.*

1. Introduction

At present, processes involving metastable electronically excited molecules of singlet oxygen (SO) $O_2(a^1\Delta_g)$ attract considerable interest. This is due to the fact that SO possesses a very long radiative lifetime (~ 4500 s) and extremely low rates of nonresonance deactivation, making it possible to produce a nonequilibrium energy stock in an $O_2(a^1\Delta_g)$-containing medium and preserve it over a long period of time. Not only does this property of SO play an important part in different fields of science, such as low-temperature plasma physics, biology, atmosphere physics etc., but it is also employed in laser technology. The most spectacular example is an oxygen – iodine laser (OIL) [1, 2]. The operation of this laser is based on the resonance transfer of excitation energy from $O_2(a^1\Delta_g)$ molecules to iodine atoms $I(^2P_{1/2})$

$$O_2(a^1\Delta_g) + I(^2P_{3/2}) \underset{k^-}{\overset{k^+}{\rightleftarrows}} O_2(X\,^3\Sigma_g^-) + I(^2P_{1/2}) + 400\ \text{K}, \quad (1)$$

O.V. Braginskii, A.N. Vasil'eva, K.S. Klopovskii, A.S. Kovalev, D.V. Lopaev, Yu.A. Mankelevich, N.A. Popov, A.T. Rakhimov, T.V. Rakhimova D.V. Skobel'tsyn Institute of Nuclear Physics, M.V. Lomonosov Moscow State University, Vorob'evy gory, 119992 Moscow, Russia; e-mail: kovalev@dnph.phys.msu.su, trakhimova@mics.msu.su

Received 13 September 2004
Kvantovaya Elektronika **35** (1) 21 – 26 (2005)
Translated by E.N. Ragozin

where $k^+ = 7.6 \times 10^{-11}$ cm^3 s^{-1} is the rate constant of the direct process at 300 K [1] and $k^- = 2.67 \times 10^{-11}$ cm^3 s^{-1} is the rate constant for the inverse process [1, 2]. The population inversion between the $I(^2P_{1/2})$ and $I(^2P_{3/2})$ levels of atomic iodine is achieved when the $O_2(a^1\Delta_g)$ yield is

$$\eta = \frac{[O_2(a^1\Delta_g)]}{[O_2(a^1\Delta_g)] + [O_2]} > \frac{1}{1 + 2k_{eq}}, \quad (2)$$

where

$$k_{eq} = \frac{3}{4}\exp\left(\frac{400}{T_g}\right) \quad (3)$$

is the equilibrium constant for the process (1). At the temperature $T_g = 300$ K, the SO yield $\eta = [O_2(a^1\Delta_g)] \times ([O_2(a^1\Delta_g)] + [O_2])^{-1}$ should exceed 0.15. In a chemical OIL, the $O_2(a^1\Delta_g)$ molecules are chemically produced in a reactor, as a rule, in the gas – liquid reaction of chlorination of the solution of alkali and hydrogen peroxide. The gas mixture issuing from the reactor contains oxygen, water vapour, H_2O_2, and unreacted chlorine, and therefore the development of a non-chemical SO generator is of considerable interest.

It is known that SO can be efficiently excited in a gas discharge. Two conditions should be fulfilled to operate an electric-discharge generator of SO (EGSO). Since the SO yield required to obtain inversion in an OIL increases exponentially with increasing temperature, in the EGSO it should be rather high (~ 0.2). In this case, the absolute concentration of $O_2(a^1\Delta_g)$ should also be high (comparable to and exceeding the concentration typical for chemical OILs [1]), i.e. higher than 10^{16} cm^{-3}. It was shown [2 – 5] that radio-frequency and microwave discharges are promising tools for the excitation of SO.

In Ref. [4], we studied experimentally and theoretically the production and loss kinetics of SO in the flow of pure oxygen as well as in its mixtures with argon and helium excited by a radio-frequency discharge (13.56 MHz) in a quartz tube in broad pressure (1 – 20 Torr) and energy deposition (1 – 2000 J mmol^{-1}) ranges. It was shown that the RF discharge can exist in three regimes, depending on the energy deposition into the plasma: in the regime of homogeneous discharge between the electrodes, or in the α regime (in the α discharge regime); in a substantially inhomogeneous regime, when plasma jets are formed beyond the electrode regions (the jet regime); and in the transition $\alpha - \gamma$ regime, when bright near-electrode layers appear in the discharge. SO is most actively produced in the

α discharge regime; in this case, the energy efficiency is found to be close to 5 %. In the jet regime, the efficiency is significantly lower (1 % – 2 %) owing to considerable energy losses in the near-electrode layers, in which secondary ion emission effects come into play.

An important finding of these investigations is the saturation of the SO concentration with increasing pressure and specific energy deposition. In this case, despite the saturation of the SO concentration, the parameter $Y = [O_2(a\,^1\Delta_g)]/[O_2(X\,^3\Sigma_g^-)]$ amounted to $\sim 30\,\%$ for a low oxygen pressure (1 – 2 Torr) and a high energy deposition, i.e. in the jet discharge regime.

A detailed investigation of the production and loss of SO in the α regime carried out on the basis of an elaborate self-consistent discharge model allowed us to elucidate the reason why the SO yield saturated with pressure. It was shown that this effect is caused by a rapid $O_2(a\,^1\Delta_g)$ quenching in the reaction

$$O(^3P) + O_2(a\,^1\Delta_g) + O_2 \rightarrow 2O_2 + O(^3P). \qquad (4)$$

By comparing the experimental and numerical data on the $O_2(a\,^1\Delta_g)$ quenching kinetics, we estimated the rate constants for this process as $k_4 \sim 10^{-32}$ cm^{6}s^{-1}.

The progress in the employment of electric-discharge SO excitation in an OIL is associated primarily with the possibility of increasing the pressure of the active medium. In this connection the aim of our work is to investigate the kinetics of SO saturation in an RF discharge in oxygen and to try for new ways of eliminating the effect of the SO concentration saturation. The investigation was carried out in the transition $\alpha - \gamma$ regime, when the specific energy deposition in the plasma is already relatively high (from 100 to 300 J mmol^{-1}) and the inefficient jet regime is not yet realised and the energy efficiency of $O_2(a\,^1\Delta_g)$ excitation is rather high ($\sim 3\,\%$). The pressure range under investigation was 4 – 20 Torr.

Since the SO concentration saturation is determined by the process (1), to eliminate the saturation requires removing atomic oxygen from the gas mixture. As determined earlier in RF discharge experiments, the main process responsible for the loss of the atoms throughout the pressure range under investigation is their heterogeneous recombination at the walls of the quartz discharge tube [4]. It is well known that the probability of surface recombination of the $O(^3P)$ atoms with the oxides of some metals (for instance, HgO, AgO, etc.) is rather high. That is why the walls of the discharge tube were coated with mercury oxide HgO to remove atomic oxygen.

2. Experiment

Figure 1 shows the scheme of the setup for producing a RF discharge. The discharge was initiated in the flow of pure oxygen in 1-m long quartz tube with an internal diameter of 14 mm by using RF generator (*1*) with a power up to 200 W operating at a frequency of 13.56 MHz. The generated power was delivered via a matching device to two 30-cm long water-cooled electrodes located outside the tube. A special spacer provided the thermal contact between the electrodes and the tube. Therefore, the discharge tube was also cooled with the aid of the electrodes. An RF measuring system furnished measurements of the incident and reflected wave amplitudes as well as of the voltage across the electrodes, the discharge current, and the angle of phase shift between them. This allowed us to monitor the RF power deposited into the gas with a good accuracy. The gas evacuation system provided a gas flow velocity in the tube up to 12 m s^{-1} for a pressure up to 40 Torr. The gas pressure was monitored by two deformation sensors at the inlet and outlet of the tube. The gas and tube surface temperatures were determined with the aid of thermocouples translatable along the tube length.

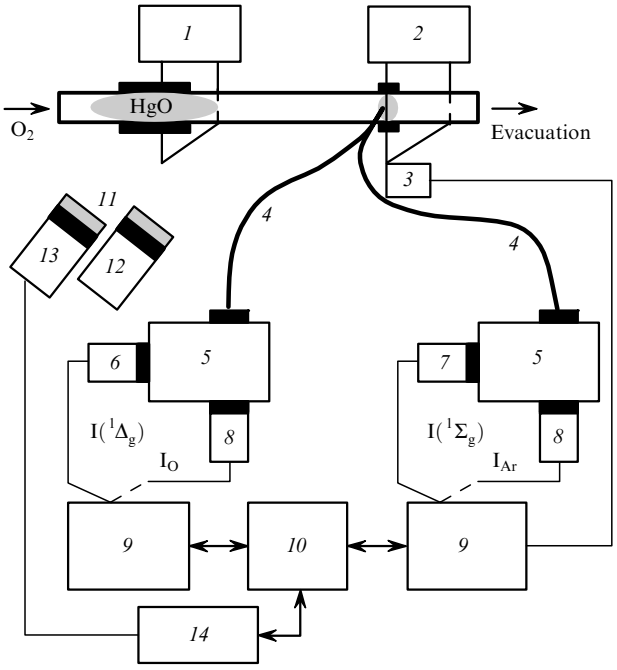

Figure 1. Scheme of the setup for obtaining a transverse RF discharge: (*1*) main RF generator; (*2*) auxiliary RF generator (40 MHz, 1-cm long electrodes); (*3*) measuring system, which determines the position of optical fibre relative to the main RF discharge electrodes; (*4*) two-channel optical fibre; (*5*) monochromators; (*6*) Ge detector cooled by liquid nitrogen; (*7*) photomultiplier for recording the radiation of $O_2(b\,^1\Sigma_g^+)$ molecules; (*8*) photomultiplier for recording the radiation of atomic oxygen [$O(^5P) \rightarrow O(^5S)$, $\lambda = 777$ nm] and argon [$Ar(2p_1) \rightarrow Ar(1s_2)$, $\lambda = 750$ nm]; (*9*) synchronous detectors; (*10*) computer; (*11*) interference filters; (*12*) absolute radiation power radiometer; (*13*) ICCD camera; (*14*) ICCD controller.

The concentration of oxygen molecules which were in the metastable states $a\,^1\Delta_g$ and $b\,^1\Sigma_g^+$ were measured along the gas flow as functions of the transport time by emission spectroscopy technique from the absolute emission intensities of the transitions $O_2(a\,^1\Delta_g, v = 0) \rightarrow O_2(X\,^3\Sigma_g^-, v = 0)$ ($\lambda = 1268$ nm) and $O_2(b\,^1\Sigma_g^+, v = 0) \rightarrow O_2(X\,^3\Sigma_g^-, v = 0)$ ($\lambda = 762$ nm), respectively. The emission from the tube section selected by a system of apertures was focused onto the input of two-channel optical fibre (*4*), providing two independent optical measuring channels. This optical system was assembled on platform (*3*) translatable along the tube length, which allowed us to measure the concentrations of excited particles at different distances from the discharge.

The radiation in both channels was modulated and directed to the entrance slits of monochromators (*5*). Ge detector (*6*) cooled by liquid nitrogen was placed at the exit slit of the first monochromator employed to record emission

from the $O_2(a\,^1\Delta_g)$ molecules. IR photomultiplier (*7*) was placed at the exit slit of the second monochromator for the simultaneous recording of emission from the $O_2(b\,^1\Sigma_g^+)$ molecules. The output signals from both photodetectors were fed to synchronous detectors (*9*) controlled by personal computer (*10*). In addition, the signal about the position of optical system (*3*) relative to the RF discharge electrodes was fed to ADC of one of the synchronous detectors. The sensitivity of this optical system provided the measurement of concentrations of $O_2(a\,^1\Delta_g)$ molecules and $O_2(b\,^1\Sigma_g^+)$ molecules down to $(2-3)\times 10^{13}$ cm^{-3} and 10^{10} cm^{-3}, respectively.

Oxygen atoms in the $O(^3P)$ ground state were detected by the method of actinometry by argon atoms. We employed the $O(^5P) \rightarrow O(^5S)$ transitions at 777 nm and the $Ar(2p_1) \rightarrow Ar(1s_2)$ transition at 750 nm, for which the cross sections for electron excitation and collisional deactivation rates are known well enough, making it possible to obtain reliable results about the concentration of atomic oxygen at high pressures. This method involving two channels (monochromator–photomultiplier) was described in detail in Ref. [4]. We studied the $O(^3P)$ concentration dynamics by using ICCD system (*13*, *14*) with a set of interference filters (*11*) for the emission lines of oxygen and argon atoms. This allowed us to determine the spatial distribution of the atoms in the discharge volume with the help of a tomography algorithm similar to the Abelian transformation. This information was used to obtain the distribution of the concentration of atomic oxygen in the discharge along the gas flow.

3. Experimental results

Experiments showed that the concentration of $O_2(a\,^1\Delta_g)$ attains saturation in the interelectrode space, the characteristic time required to attain the saturation decreasing with increase in the energy deposition. Figure 2 shows the dependence of the ratio $[O(^3P)]/N$ (N is the total particle density in the discharge volume for the corresponding gas temperature) along the discharge, and Fig. 3 shows the distribution of $[O_2(a\,^1\Delta_g)]$ in pure O_2 at a pressure of 15 Torr, a flow velocity of 6.3 m s^{-1}, and an energy deposition of 190 J mmol^{-1}. One can see that even at the very beginning of the discharge, the $[O(^3P)]/N$ ratio attains its stationary value, which somewhat increases towards the discharge end. The concentration of $O_2(a\,^1\Delta_g)$ molecules reaches a maximum closer to the end of the electrodes, approximately at a distance of 15–20 cm.

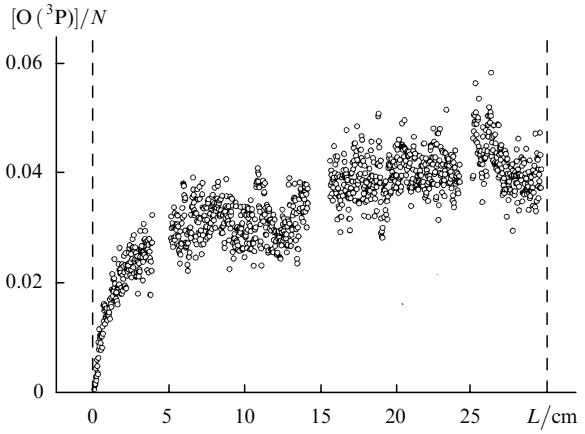

Figure 2. $[O(^3P)]/N$ ratio distribution along of the discharge (N is the total particle density in the discharge volume for the corresponding gas temperature) in pure O_2 at a pressure of 15 Torr, a flow velocity of 6.3 m s^{-1}, and an energy deposition of 190 J mmol^{-1}. The tube walls were not coated with HgO.

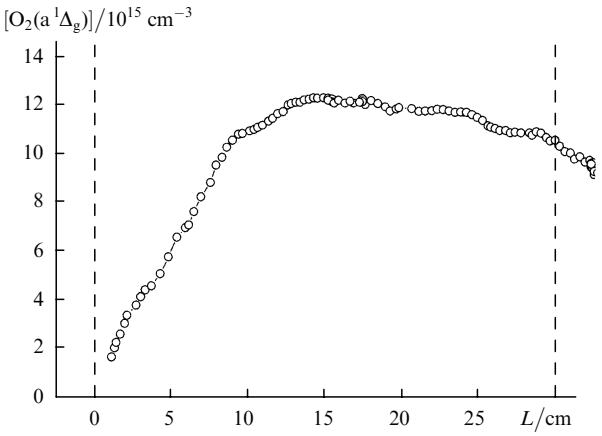

Figure 3. Distribution of $[O_2(a\,^1\Delta_g)]$ in pure O_2 for a pressure of 15 Torr, a flow velocity of 6.3 m s^{-1}, and an energy deposition of 190 J mmol^{-1}. The tube walls were not coated with HgO.

Figure 4 shows the concentrations $O_2(a\,^1\Delta_g)_{max}$ and $O_2(b\,^1\Sigma_g^+)_{max}$ as functions of specific energy deposition in the discharge in pure O_2 for pressures of 4, 7, 10, and 15 Torr and a flow velocity of 6.3 m s^{-1}. One can see that these dependences are nonmonotonic. For all pressures, the concentrations $O_2(a\,^1\Delta_g)_{max}$ and $O_2(b\,^1\Sigma_g^+)_{max}$ rather rapidly reach saturation with increasing the energy deposition and then gradually decrease. Earlier [4], when investigating the

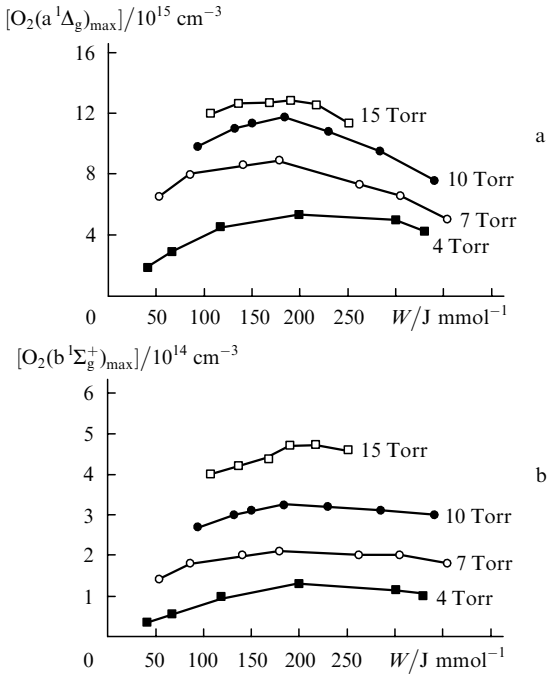

Figure 4. Maximum concentrations $O_2(a\,^1\Delta_g)_{max}$ (a) and $O_2(b\,^1\Sigma_g^+)_{max}$ (b) as functions of specific energy deposition in the discharge in pure O_2 for different pressures and a flow velocity of 6.3 m s^{-1}.

SO concentration kinetics in the afterglow of an RF discharge it was found that increasing the pressure at the post-discharge stage resulted in a rapid quenching of $O_2(a\,^1\Delta_g)$, which was impossible to describe by the presently known binary processes. On the basis of a detailed analysis and comparative calculations performed for different pressures it was established that the resultant experimental data on the transport dynamics of SO could be explained only assuming a three-body mechanism of $O_2(a\,^1\Delta_g)$ deactivation by oxygen atoms in the process (4) with the rate constant of $\sim 10^{-32}$ cm^6 s^{-1}.

In order to remove atomic oxygen, the walls of the discharge tube were coated with mercury oxide in the electrode region. Figure 5 shows the dependences of the concentration $O_2(a\,^1\Delta_g)_{max}$ on the energy deposition in the discharge, similar to the dependences plotted in Fig. 4. In experiments with HgO, the SO concentration was measured in the afterglow of the discharge. It was found that, for a flow velocity of ~ 6 m s^{-1} the concentration $O_2(a\,^1\Delta_g)_{max}$ remained almost invariable up to a distance of 20 cm from the end of the electrodes. One can see that the removal of atomic oxygen had a different effect on the characteristic form of the dependences $[O_2(a\,^1\Delta_g)_{max}](W)$ for different pressures. The most significant results is that in the region of existence of the α and transition $\alpha-\gamma$ regimes there occurs no $O_2(a\,^1\Delta_g)$ concentration saturation with increasing power deposition in the plasma. In this case, the value of Y for a pressure $p = 10-15$ Torr amounts to 10 %–12 % and is limited only by the RF generator power.

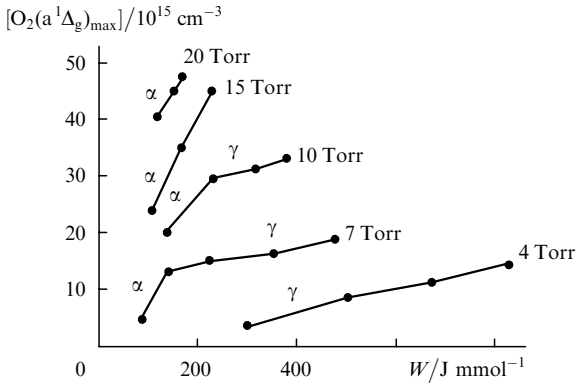

Figure 5. Maximum concentrations $O_2(a\,^1\Delta_g)_{max}$ as a function of specific energy deposition in the discharge (the α and $\alpha-\gamma$ regimes) in pure O_2 for different pressures and a flow velocity of 6.3 m s^{-1}. The tube walls are coated with HgO.

Obtaining a high SO concentration by using HgO allowed us to record the $O_2(a\,^1\Delta_g)$ dynamics also from the $O_4(^1B_{2u}) \rightarrow O_4(^1A_g)$ dimole transition radiation arising due to collisions of two $O_2(a\,^1\Delta_g)$ molecules:

$$O_2(a\,^1\Delta_g, v=0) + O_2(a\,^1\Delta_g, v=0)$$

$$\rightarrow O_2(X\,^3\Sigma_g^-, v=0) + O_2(X\,^3\Sigma_g^-, v=0),\ \lambda = 635\ \text{nm},$$

$$O_2(a\,^1\Delta_g, v=0) + O_2(a\,^1\Delta_g, v=0)$$

$$\rightarrow O_2(X\,^3\Sigma_g^-, v=0) + O_2(X\,^3\Sigma_g^-, v=1),\ \lambda = 703\ \text{nm}.$$

Figure 6 shows a typical afterglow spectrum of the RF discharge in pure oxygen at a pressure of 15 Torr, a flow velocity of 3 m s^{-1}, and an energy deposition of 450 J mmol^{-1} at a distance of 20 cm from the electrode end. The inset shows for comparison the same spectrum together with the well-known $O_2(b\,^1\Sigma_g^+, v=0) \rightarrow O_2(X\,^3\Sigma_g^-, v=0)$ transition at 762 nm. This spectrum is completely similar to the spectrum observed in chemical SO generators. The dimole radiation of SO was strong enough for the red radiation of the discharge afterglow to be visually

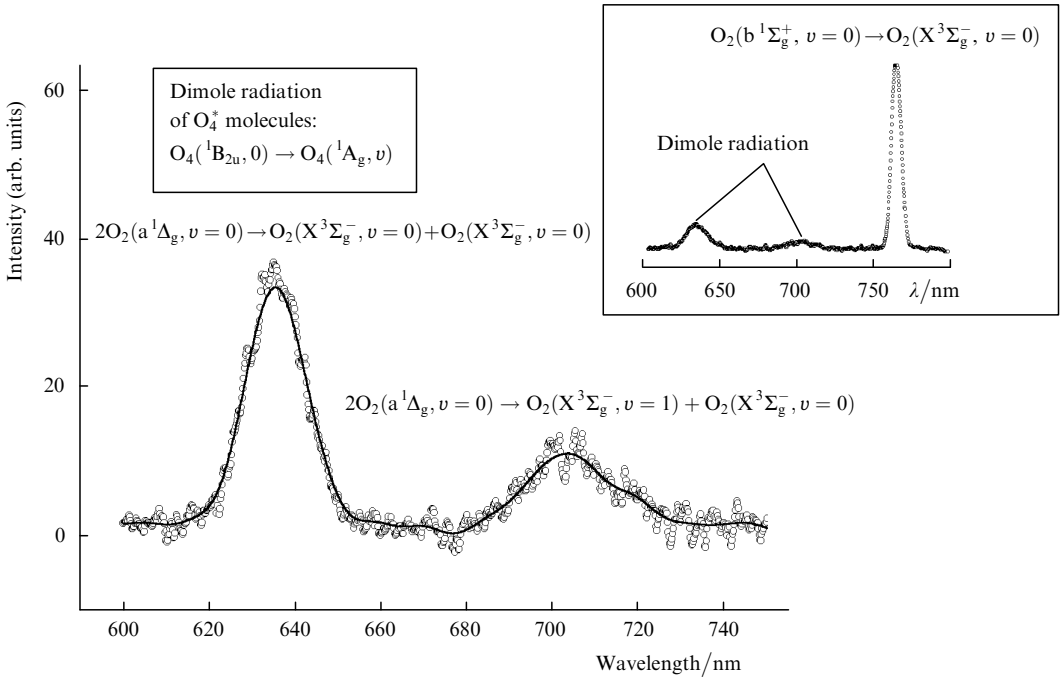

Figure 6. Typical afterglow spectrum of the RF discharge in pure oxygen for a pressure of 15 Torr, a flow velocity of 3 m s^{-1}, and an energy deposition of 450 J mmol^{-1} at a distance of 20 cm from the electrode end.

observed in the dark. Moreover, the dimole radiation power also turned out to be high enough, and it was possible to measure it directly with the help of an absolute power radiometer. This allowed us to check the accuracy of the absolute $O_2(a^1\Delta_g)$ concentration measurements.

Figure 7 shows the dependences of the maximum concentration $O_2(a^1\Delta_g)_{max}$ on the energy deposition for an oxygen pressure of 15 Torr and a flow velocity of 3 m s^{-1}. These data were obtained from intensity measurements of the radiation arising from the $O_2(a^1\Delta_g,\ v=0) \rightarrow O_2(X^3\Sigma_g^-, v=0)$ at 1270 nm (after absolute calibration) and from direct power measurements of the dimole radiation at 635 nm. Taking into account the calibration accuracy [±25 % (1270 nm) and ±15 % (635 nm)], both measurements yield the same result, which testifies to the correctness of the data obtained.

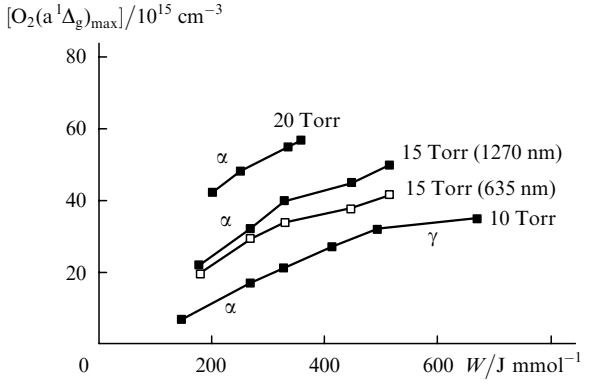

Figure 7. Dependences of maximum concentration $O_2(a^1\Delta_g)_{max}$ on the energy deposition for an oxygen pressure of 15 Torr and a flow velocity of 3 m s^{-1} obtained from intensity measurements of the radiation arising from the $O_2(a^1\Delta_g, v=0) \rightarrow O_2(X^3\Sigma_g^-, v=0)$ at $\lambda = 1270$ nm and from direct power measurements of the dimole radiation at $\lambda = 635$ nm. The tube walls are coated with HgO.

4. Discussion of results

From a comparison of the experimental data shown in Figs 4a and 5 one can draw the following conclusions. Figure 5 shows that the dependences of the SO concentration on the energy deposition W in the experiments with HgO are not saturated, as was the case in the absence of mercury oxide. However, their slope changes beginning with some value of W specific for each pressure. This testifies to a possible structural change of the RF discharge. Namely, the discharge gradually passes to the $\alpha - \gamma$ regime, which is much less efficient from the standpoint of SO excitation than the α regime [4].

A comparison of the maximum concentrations $O_2(a^1\Delta_g)_{max}$ obtained in the discharge in the absence of mercury oxide (Fig. 4a) with the data obtained with the use of HgO (Fig. 5) shows that the $O_2(a^1\Delta_g)$ concentration in experiments with HgO increases by about a factor of 2–2.5 for $p > 10$ Torr and $W = 100 - 200$ J $mmol^{-1}$. This suggests that the $O_2(a^1\Delta_g)$ concentration saturation in the discharge is caused by the quenching of this molecule by atomic oxygen [see the reaction (4)].

We analysed and simulated the experimental data by using a self-consistent model of the RF discharge α mode [4]. The calculated distributions of the $O_2(a^1\Delta_g)$ and $O(^3P)$ concentrations and the $[O(^3P)]/N$ ratio in the discharge without HgO for an oxygen pressure of 15 Torr, an energy deposition of 190 J $mmol^{-1}$, and a flow velocity of 6.3 m s^{-1} are given in Fig. 8a. A similar calculation in the presence of mercury oxide on the tube walls is shown in Fig. 8b. To model the dynamics of the $[O(^3P)]/N$ ratio in the discharge, we employed an expression for the probability γ_0 that an atom is lost at the hot quartz surface. This expression is an approximation of our experimental data obtained in the dc glow discharge in the tube [6]: $\gamma_0 = 1.5 \times 10^{-3}(0.5 + 1.7)A[O(^3P)]/4 \times 10^{15})$, where $A = 1$ for $p \leqslant 5$ Torr and $A = 5/p$ for $p > 5$ Torr. In the case of a cooled surface, i.e., for $T_w \approx 280$ K, the coefficient by the parentheses was taken to be equal to 0.5×10^{-3}. This value is in good agreement with the data of our experiment in the dc discharge for a pressure higher than 3 Torr and a cooled wall [6] as well as with the data of Refs [7, 8].

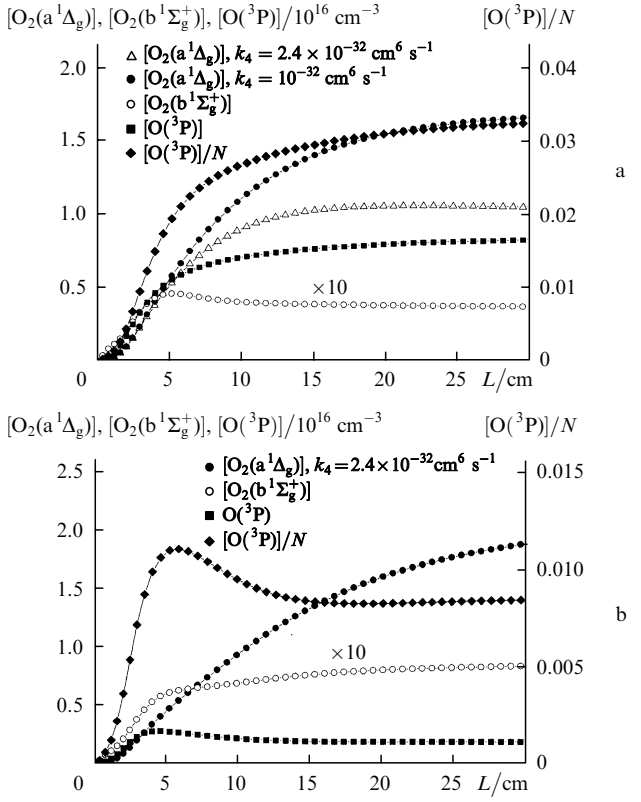

Figure 8. Calculated $O_2(a^1\Delta_g)$-, $O_2(b^1\Sigma_g^+)$-, and $O(^3P)$-concentration and $[O(^3P)]/N$-ratio distributions lengthwise of the discharge for an oxygen pressure of 15 Torr, an energy deposition of 190 J $mmol^{-1}$, and a flow velocity of 6.3 m s^{-1} without (a) and with (b) the HgO coating.

A comparison of Figs 4a and 8a shows that the experimental results are adequately described by the calculated values of the $[O(^3P)]/N$ ratio. The calculations suggest that the main process responsible for the production of atomic oxygen is the dissociation of the O_2 molecules by electron impact in the processes

$$e + O_2(X^3\Sigma_g^-) \rightarrow e + O(^3P) + O(^3P), \quad (5)$$

$$e + O_2(X^3\Sigma_g^-) \rightarrow e + O(^3P) + O(^1D), \quad (6)$$

where $O_2(X^3\Sigma_g^-)$ are the O_2 molecules in the ground

electronic state. The principal channel for the loss of oxygen atoms is their heterogeneous recombination at the surface of the quartz tube with a characteristic time $\tau_w \sim 10$ ms, which is determined by the characteristic frequencies of atomic diffusion and recombination at the surface. The conversion of atomic oxygen to ozone makes only a small contribution to the loss of the atoms. Note that in a 1D model with a constant transit velocity v_f it is difficult to take into account the real radial velocity distribution of the gas flow $v(r) = 2v_0(1 - r^2/R^2)$, where v_0 is the average flow velocity and R is the tube radius. Considering that the characteristic time of radial particle diffusion is shorter than the time of particle transit through the discharge region, the attainment of stationary $[O(^3P)]/N$ and $[O_2(a\,^1\Delta_g)]$ distributions as well as the experimental energy deposition for a given RF voltage at the electrode are more adequately described using the velocities of near-wall flows rather than the average velocity v_0. In the calculations reported, we used the value $v_f = 0.4v_0$. In this case, the calculated specific energy deposition was equal to about 190 J mmol^{-1}.

We now compare the experimental and calculated data on the $O_2(a\,^1\Delta_g)$ concentration distribution along the discharge. One can see from Fig. 8a that, despite the good agreement between the results of calculation and the experimental data on the $[O(^3P)]/N$ ratio, the calculated $O_2(a\,^1\Delta_g)$ concentration increases somewhat slower than the experimental one, and the concentration of SO turns out to be higher by the end of discharge. Our calculations suggest that the main process responsible for the production of $O_2(a\,^1\Delta_g)$ is the excitation of oxygen by direct electron impact,

$$e + O_2(X\,^3\Sigma_g^-) \rightarrow e + O_2(a\,^1\Delta_g), \quad (7)$$

and the attainment of saturation is primarily determined by the three-body deactivation (4). The rates of quenching of the $O_2(a\,^1\Delta_g)$ molecules in the course of the two-particle reaction involving atomic oxygen due to hyperelastic collisions are approximately two times lower.

Note that we used in this calculation the rate constant for reaction (4) proposed in Ref. [4]. However, as noted in Ref. [4], the process (4) is multistage, and it is quite probable that this rate constant, as the 'gross' of the process, does not provide an equally adequate description of all its stages under different conditions and exhibits a nontrivial dependence on the gas temperature. By way of illustration, Fig. 8a shows the $[O_2(a\,^1\Delta_g)]$ distribution calculated for $k_4 = 2 \times 10^{-32}$ cm^6 s^{-1}. One can see that a two-fold increase in k_4 provides a rather good reproduction of both the form of $O_2(a\,^1\Delta_g)$ concentration distribution and its maximum value, which also corresponds to the experimental data obtained for the dimole radiation of $O_2(a\,^1\Delta_g)$.

Calculations for the conditions of Fig. 8a but with the HgO coating of the tube walls (in the model it was assumed that this corresponds to $\gamma_0 = 1$) are given in Fig. 8b. They were performed for $k_4 = 2.4 \times 10^{-32}$ cm^6 s^{-1}. One can see that the $O_2(a\,^1\Delta_g)$ concentration increases two-fold on removal of atomic oxygen in comparison with the concentration of SO without HgO. Interestingly, the calculated $[O_2(a\,^1\Delta_g)]$ distribution in the discharge exhibits a weak saturation, which is due to impacts of the second kind. The increase in the $O_2(a\,^1\Delta_g)$ concentration after discharge early in the afterglow reflects the increase in the gas density due to the dynamics of the gas temperature. Note that the SO concentration rose by about a factor of three in the experiment with the use of HgO under similar conditions. The 1.5-fold difference between the experimental and calculated values of $O_2(a\,^1\Delta_g)_{max}$ with the use of HgO shows that higher, on the average, electron temperatures ($T_e > 2.2$ eV) are realised under real experimental conditions.

Therefore, the results of this work demonstrate the feasibility of obtaining a high SO yield in high-pressure RF discharges. In particular, the yield of SO for an oxygen pressure of 15 Torr is ~ 10 %.

5. Conclusions

We have studied experimentally and theoretically the excitation of SO in $O_2(a\,^1\Delta_g)$ in the α and intermediate $\alpha - \gamma$ regimes of an RF discharge at a frequency of 13.56 MHz.

Experiments were carried out on the heterogeneous removal of oxygen atoms from the surface of the discharge tube coated with mercury oxide HgO. It was shown that the decrease in the concentration of the atomic oxygen in the discharge results in an increase in the density of the $O_2(a\,^1\Delta_g)$ molecules by about a factor of 2–2.5 for an oxygen pressure above 10 Torr. High SO yields (~ 10 %) were obtained for the discharge at a pressure of 15 Torr.

Acknowledgements. This work was supported by the International Science and Technology Centre (Grant No. 1581), a grant of the President of Russia (No. NSh-1713.2003.2), and the Russian Foundation for Basic Research (Grant No. 03-02-16925).

References

1. Yuryshev N.N. *Kvantovaya Elektron.*, **23**, 583 (1996) [*Quantum Electron.*, **26**, 567 (1996)].
2. Fujii H., Itam S., Kihara Y., et. al. *Proc. SPIE Int. Soc. Opt. Eng.*, **4065**, 818 (2000).
3. Carroll D.L., King D.M., Verdeyen J.T., Woodard B., Zimmerman J., Skorski L., Solomon W.C. *AIAA Paper*, **4029** (2003).
4. Rakhimova T.V., Kovalev A.S., Rakhimov A.T., Klopovsky K.S., Lopaev D.V., Mankelevich Yu.A., Proshina O.V., Braginsky O.V., Vasilieva A.N. *AIAA Paper*, **4306** (2003).
5. Savin Yu.V., Goryachev L.V., Adamenkov A.A., Adamenkov Yu.A., Ilyin S.P., Kolobyanin Yu.V., Kudryashov E.A., Vyskubenko B.A., Rakhimova T.V., Mankelevich Yu.A., Popov N.A. *AIAA Paper*, **4305** (2003).
6. Lopaev D.V., Smirnov A.V. *Proc. ISTAPC-2002*, **1**, 213 (2002).
7. Kim Y.C., Boudart M. *Langmuir*, **7**, 2999 (1991).
8. Cartry G., Magne L., Cernogira G. *J. Phys. D: Appl. Phys.*, **32**, 1894 (1999).